Title	Thermal-diffusivity measurements of an oriented superconducting-film–substrate composite using the mirage technique
Author(s)	Wong, PK; Fung, PCW; Tam, HL; Gao, J
Citation	Physical Review B (Condensed Matter), 1995, v. 51 n. 1, p. 523-533
Issued Date	1995
URL	http://hdl.handle.net/10722/43233
Rights	Creative Commons: Attribution 3.0 Hong Kong License

Thermal-diffusivity measurements of an oriented superconducting-film–substrate composite using the mirage technique

P. K. Wong, P. C. W. Fung, H. L. Tam, and J. Gao
Physics Department, The University of Hong Kong, Hong Kong
(Received 15 April 1994)

When one measures the thermal diffusivity χ of a thin film on a substrate by the mirage method, the photothermal deflection of the probe beam is caused by the heat field contributed by both the film and the substrate which are heated by the pump beam. To include the effects due to the presence of the substrate, we present a method to measure the diffusivities of both the film and substrate in one set of mirage detection. Using the off-axis magnetron sputtering process, we fabricated $YBa_2Cu_3O_{7-\delta}$ thin films of suitable thickness ($\sim$60 nm) on $SrTiO_3$ as our sample for χ measurements along the c and b axes. Our results are consistent with published ones.

I. INTRODUCTION

Specific-heat and thermal-diffusivity measurements give significant information on the occurrence of phase transition.[1] Moreover, since the strength of interaction between lattice phonons and electrons will affect the observed diffusivity, thermal analysis of crystals can in some cases bridge microscopic and macroscopic properties. In fact, analysis of thermal diffusivity is one of the basic means used to give a crucial clue as to whether high-T_c ceramic superconductivity has its origin in phonon-electron interaction. Moreover, since most superconducting crystals have an anisotropic lattice structure, and consequently anisotropic diffusivity coefficients, crystal structure is related to observed diffusivity if the sample is a single crystal. On the application side, we need to know the thermal diffusivity of the materials used in making microelectronic components in order to optimize the operation in many cases.

Needless to say, the calorimetric method is not accurate enough to measure thermal diffusivity of materials with low diffusivity and heat capacity, such as thin superconducting films. "Nondestructive" methods have been introduced to measure the diffusivity of crystals, which may have low diffusivity coefficients. However, some part of the sample has to be brought in contact with certain measuring devices using such methods. For example, the samples need to be in contact with the heating mechanisms and/or the transducers or thermometers.[2] Until very recently, the transient grating (TG) method was modified[3] and applied to measure the anisotropic thermal diffusivity of $YBa_2Cu_3O_{7-\delta}$ thin film in 1993.[4,5] We would note here that previous analysis of the TG method before 1991 accepted the assumption that the gratings were spatially uniform or slowly varying along the normal of the sample surface[6] compared with the probe wavelength. Therefore, the standard TG method was restricted to the measurement of weakly absorbing or nonabsorbing samples. A more general treatment considering spatially nonuniform gratings was reported in 1991.[3] Indeed, a more advanced version of TG was then introduced to measure the thermal diffusivity of $YBa_2Cu_3O_{7-\delta}$ thin film.[4,5] In such experimentation, a dye-laser pulse was split into three pulses with similar intensities. Two of the pulses were focused and crossed inside the film to excite a grating with a wave vector perpendicular to the surface normal. The third pulse was suitably delayed to act as the probe beam. The associated theory predicts that the temporal change of diffraction efficiency η of both transmission and reflection geometries can be expressed as $\eta \propto \exp(-2D\beta^2 t)$,[4,5] where D and β are the thermal diffusivity parallel to the film surface and the wave vector of the grating, respectively. The thermal diffusivity was obtained by numerically fitting the theoretical expression of $\eta(t)$. Though the method is really "noncontacting," it is very difficult to set up the experimental optically and under a vacuum of 10^{-6} Torr. Moreover, a number of parameters must be known before the stated numerical fitting can be carried out to evaluate the thermal diffusivity.

Even before the advent of the TG method, the noncontacting mirage technique had already been established.[7–10] While unoriented films are very suitable samples using the mirage method, the thin film must be attached to the substrate. In other words, the true sample is a film-substrate composite as a whole. If the film is very thin, a significant portion of the pump power will be absorbed by the substrate, and the thermal wave, thus originated, will reach the field position where the probe is passing. In the past, theoretical analysis has not taken into account the heat field generated by the substrate, rendering the deduced diffusivity coefficient questionable if the film is thin and is composed of material with low thermal diffusivity.

Based on the above considerations, the objectives of this investigation are the following. (i) Derive an explicit expression of the thermal diffusivity for the mirage experiment in terms of directly measurable quantities for the situation where the sample is composed of a substrate and a film, adding a new dimension to the theoretical aspect of this problem. In fact, we shall present a method in Sec. II via which we can calculate the thermal

0163-1829/95/51(1)/523(11)/$06.00

diffusivity coefficients of the film as well as the substrate by supplying data from experimentation using the mirage technique. (ii) Since our theoretical deduction shows that we must have a relatively thin film (<100 nm) within the framework of the proposed theory, we fabricate our own $YBa_2Cu_3O_{7-\delta}$ thin-film sample with a thickness of 60 nm, employing the off-axis magnetron sputtering technique. Moreover, this thickness of 60 nm on (305) $SrTiO_3$ is smaller than that (~ 200 nm) of the samples used in the TG experiments reported,[3,4] rendering our analysis (in Sec. V) more meaningful. The film has a rather uniform ratio of Y:Ba:Cu=1:2:3 throughout the film surface according to the energy dispersive x-ray analysis (EDX) experiment. We believe that it is a single-crystal thin film. (iii) We then carry out the mirage experiment along the c and b axes of the sample. Application of the theory to this particular sample is carried out, leading to the evaluation of both the thermal diffusivities of the film and that of the $SrTiO_3$ substrate. (iv) In order to check our theory further, we repeat the photothermal experiments using a pure iron slab sample as well as another iron sample with an oxidized film on top. (v) Analyze the diffusivity results of the $YBa_2Cu_3O_{7-\delta}$ material reported by others together with our findings here. (vi) Check again the origin of high-T_c Y-123 superconductivity—the low diffusivity along the c axis obtained by our combined theoretical and experimental analysis is supportive of the phonon-mediated nature of superconductivity.

II. THE HEAT FIELD OF A FILM-SUBSTRATE COMPOSITE

When a sinusoidally modulated laser beam incidents normally on a thin-film sample, a temperature distribution is established on the film surface, resulting in a refractive index gradient field within a thin layer of air in the neighborhood above the film. If a probe laser beam traverses this air layer, the deflection Φ is given by the following according to the well-known mirage effect:[11]

$$\Phi=\frac{1}{n_0}\frac{\partial n}{\partial T}\int_{\text{path}}\nabla_{\perp}T(r,t)ds\ , \tag{1}$$

where $\nabla_{\perp}T(r,t)$ is the spatial gradient of the temperature field $T(r,t)$ perpendicular to the probe beam path, n is the refractive index of air, and n_0 is that at ambient temperature.

With reference to the geometry system of Fig. 1, the temperature field on the surface of a homogeneous bulk sample is[12]

$$T(x,y_0,z=0,t)=T_0\exp\left[-\frac{y_0}{l_T}\right]\cos\left[\omega t-\frac{y_0}{l_T}\right]\ , \tag{2}$$

where $T_0=T(x,y_0=0,z=0,t=0)$, y_0 is the displacement of the probe beam from the pump beam center, and ω is the angular frequency of the pump beam. Here $l_T=(2\chi/\omega)^{1/2}$ is the thermal diffusion length, while χ is the thermal diffusivity of the sample. The surface temperature field is then coupled to the probe beam through thermal wave in air. The temperature distribution along the path of the probe beam is then (Fig. 1)

$$T(x,y_0,z=z_0,t)=T_0\exp\left[-\frac{y_0}{l_T}-\frac{z_0}{l_{0T}}\right]\times\cos\left[\omega t-\frac{y_0}{l_T}-\frac{z_0}{l_{0T}}\right]\ , \tag{3}$$

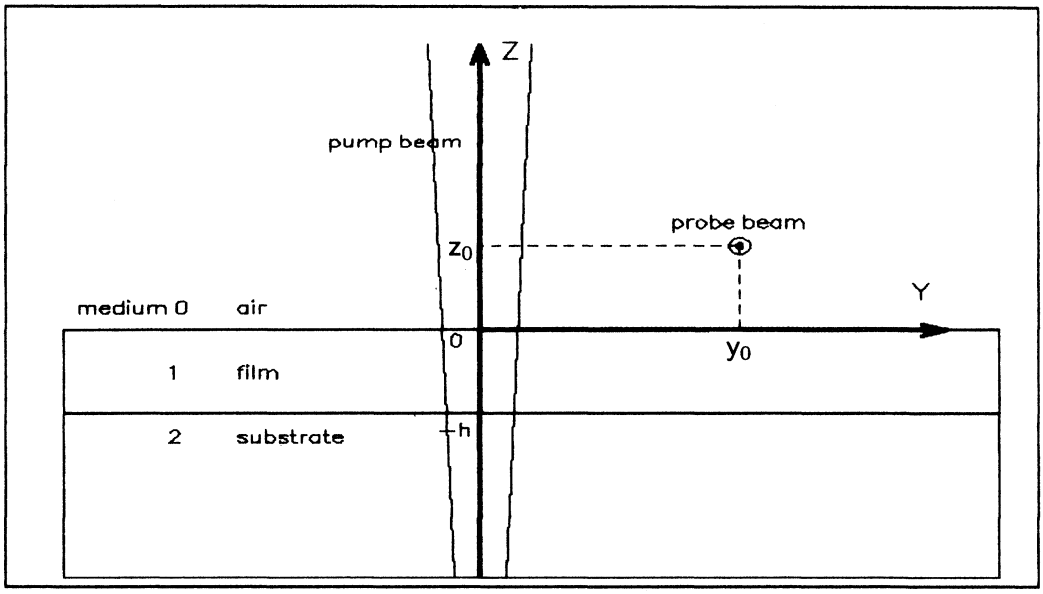

FIG. 1. Positions of the composite sample, the pump, and probe beams. The probe beam propagates along the x direction at (y_0,z_0). h is the thickness of the film.

where l_{0T} is the thermal diffusion length of air. The additional term z_0/l_{0T} in T due to thermal wave in air can be measured by recording the phase and amplitude of Φ for various values of z_0. If the deflection is relatively small, it has been shown theoretically[12] that Eq. (1) has an explicit solution:

$$\Phi=\Phi_0 \exp\left[-\frac{y_0}{l_T}-\frac{z_0}{l_{0T}}\right]\cos\left[\omega t-\frac{y_0}{l_T}-\frac{z_0}{l_{0T}}+\zeta\right] \quad (4)$$

where ζ is a constant resulting from calculation. The phase of Φ is then simply

$$\text{phase}(\Phi)=\left[-\frac{y_0}{\chi^{1/2}}-\frac{z_0}{\chi_0^{1/2}}\right](\pi f)^{1/2}+\zeta\ , \quad (5)$$

where $\omega=2\pi f$ and χ_0 is the thermal diffusivity of air. Obviously, if χ_0, y_0, and z_0 are known, χ can be obtained from the slope of the phase $(\Phi)-f^{1/2}$ plot. Since it is difficult to measure y_0 and z_0, suppose we perform the measurement at y_0 and $y_0+\Delta y_0$, and the difference between the two slopes of phase $(\Phi)-f^{1/2}$ plots as Δ slope; then it is easy to show that χ can simply be expressed as

$$\chi=\frac{\pi\Delta y_0^2}{(\Delta\ \text{slope})^2}\ . \quad (6)$$

Δy_0 in Eq. (6) can usually be measured accurately. Clearly if $(\Delta$ slope$)^2$ is large, χ is small. For an accurate result, the difference of the stated two slopes must be significant, and the method just introduced is thus particularly good for samples with low thermal diffusivity, such as superconducting ceramic thin films or pellets.

It is difficult to grow single-crystal thick film with axes all aligned in known directions. If the thickness of such a film is much smaller than the optical-absorption and thermal-diffusion lengths, a significant portion of the pump laser power can penetrate into the substrate and excite a thermal wave there, which in turn contributes to the heat field in the air layer above the film surface, where the probe beam is traversing. For a film with such a small thickness, we can assume that the temperature field is formed by simply adding the field due to the film (T_{film}) and that due to the substrate (T_{subs}):

$$T(x,y_0,z=z_0,t)=T_{\text{film}}(x,y_0,z=z_0,t)+T_{\text{subs}}(x,y_0,z=z_0,t)\ . \quad (7)$$

As T_{film} is originated from absorbing the optical power of the pump beam, it should take the same form as Eq. (3), i.e.,

$$T_{\text{film}}(x,y_0,z=z_0,t)=T_1\exp\left[-\frac{y_0}{l_{1T}}-\frac{z_0}{l_{0T}}\right]\times\cos\left[\omega t-\frac{y_0}{l_{1T}}-\frac{z_0}{l_{0T}}\right]\ , \quad (8a)$$

where T_1 is a constant in the y_0, z_0, and t domains.

If the film has a thickness h much smaller than its thermal wavelength, i.e., $h\ll 2\pi l_{1T}$, we can assume T_{subs} to have a similar form, such as Eq. (8a), so that

$$T_{\text{subs}}(x,y_0,z=z_0,t)=T_2\exp\left[-\frac{y_0}{l_{2T}}-\frac{z_0}{l_{0T}}\right]\times\cos\left[\omega t-\frac{y_0}{l_{2T}}-\frac{z_0}{l_{0T}}+\zeta_2\right]\ , \quad (8b)$$

where l_{1T} (l_{2T}) is the thermal diffusion length of the film (substrate). ζ_2 must be included here, since there may, in general, be a phase difference between T_{film} and T_{subs}. Now, in view of Eqs. (1) and (7), the observed deflection of the probe beam Φ can be expressed as

$$\Phi=\Phi_{\text{film}}+\Phi_{\text{subs}} \quad (9a)$$

$$=\Phi_1\cos\left[\omega t-\frac{y_0}{l_{1T}}-\frac{z_0}{l_{0T}}+\zeta_f\right]+\Phi_2\cos\left[\omega t-\frac{y_0}{l_{2T}}-\frac{z_0}{l_{0T}}+\zeta_s\right]\ , \quad (9b)$$

where ζ_f and ζ_s are constants. As $l_{iT}=(2\chi_i/\omega)^{1/2}$ for $i=0,1,2$, the phases of both Φ_{film} and Φ_{subs} vary linearly with $f^{1/2}$:

$$\text{phase}\ (\Phi_{\text{film}})=\left[-\frac{y_0}{\chi_1^{1/2}}-\frac{z_0}{\chi_0^{1/2}}\right]\pi^{1/2}f^{1/2}+\zeta_f\ , \quad (10a)$$

$$\text{phase}\ (\Phi_{\text{subs}})=\left[-\frac{y_0}{\chi_2^{1/2}}-\frac{z_0}{\chi_0^{1/2}}\right]\pi^{1/2}f^{1/2}+\zeta_s\ . \quad (10b)$$

In Fig. 2, Φ_{film} and Φ_{subs} are represented as vectors, with magnitude $=\Phi_1,\Phi_2$ and argument = phase(Φ_{film}), phase(Φ_{subs}), respectively. The measurable quantity Φ is the resultant vector of addition. When $f^{1/2}$ varies, Φ_{film} and Φ_{subs} rotate at different speeds, and so the phase of Φ will be periodic in the $f^{1/2}$ domain. The theoretically predicted phase-$f^{1/2}$ curve will be like the solid line in Fig. 3.

In actual practice only a portion of a full period in the phase-$f^{1/2}$ is available. For example, for limited chopper frequency, we may not have information over one complete cycle. Let us refer back to Fig. 3, where A represents a certain minimum measured in experimentation. The next maximum is then B. Note that the total Φ is the only quantity measurable.

In reality, Φ_{film} and Φ_{subs} rotate with different angular speeds, resulting in the observed variation of Φ with respect to change in $f^{1/2}$. The triangle in Fig. 2 with apex 0 rotates clockwise with our convention. It is elementary to show mathematically that at point A of Fig. 3, the phase diagram of Φ should be represented by vector $\overrightarrow{OA}$ (Fig. 4), which is perpendicular to Φ_{film}. When $f^{1/2}$ is increased, the next maximum would occur at B of Fig. 3, and the phase diagram of Φ is represented by vector $\overrightarrow{OB}$ in Fig. 4, which is perpendicular to Φ_{film} again. Assume the minimum and maximum are at $A=(f_{\min}^{1/2},p_{\min})$ and $B=(f_{\min}^{1/2}+\Delta f^{1/2},p_{\max})$, respectively, in Fig. 3. Also, Φ_{film} is considered to be rotating faster than Φ_{subs}, which is the situation occurring in most

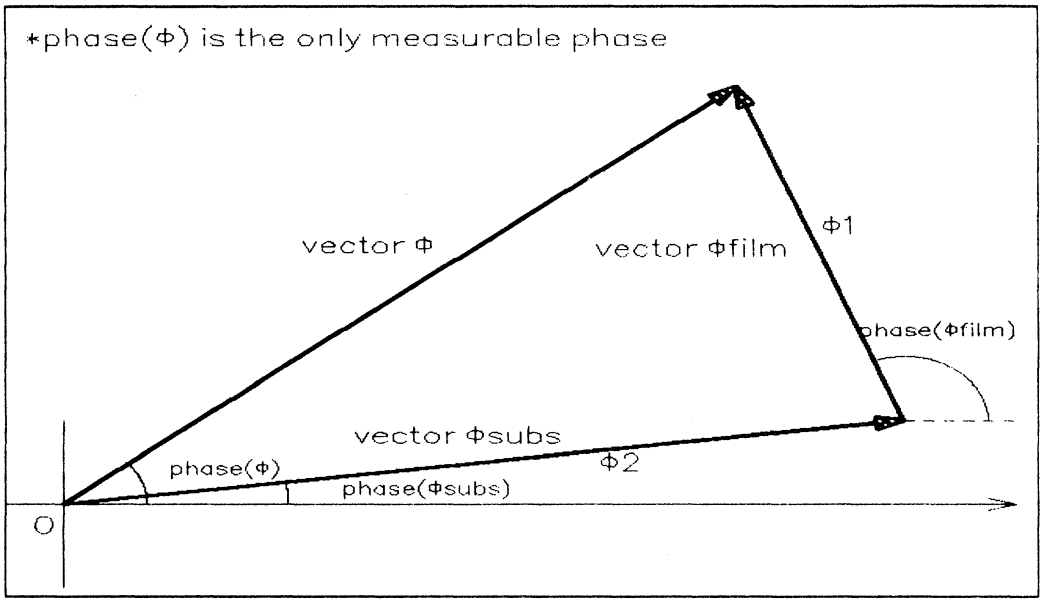

FIG. 2. The measurable deflection Φ, the deflection due to the film along Φ_{film}, and that contributed by the substrate alone Φ_{subs} are represented as vectors.

superconducting thin films. From simple geometry, we find that the phase change of Φ_{film} relative to Φ_{subs} during the interval $\Delta f^{1/2}$ is

$$-\left[\frac{\pi}{2}-\theta_{\max}\right]-\left[\frac{\pi}{2}-\theta_{\min}\right]=-\pi+\theta_{\max}+\theta_{\min}\ , \qquad (11)$$

where $\theta_{\max}$ and $\theta_{\min}$ are shown in Fig. 4. The total absolute phase change of Φ_{film} during $\Delta f^{1/2}$ is then

$$\Delta\ \text{phase}(\Phi_{\text{film}})=-\pi+\theta_{\max}+\theta_{\min}+\frac{\partial[\text{phase}(\Phi_{\text{subs}})]}{\partial(f^{1/2})}(\Delta f^{1/2})\ . \qquad (12)$$

As shown in Eqs. (10a) and (10b), phase (Φ_{subs}) and phase (Φ_{film}) are linear functions of $f^{1/2}$; we can write the above expression as

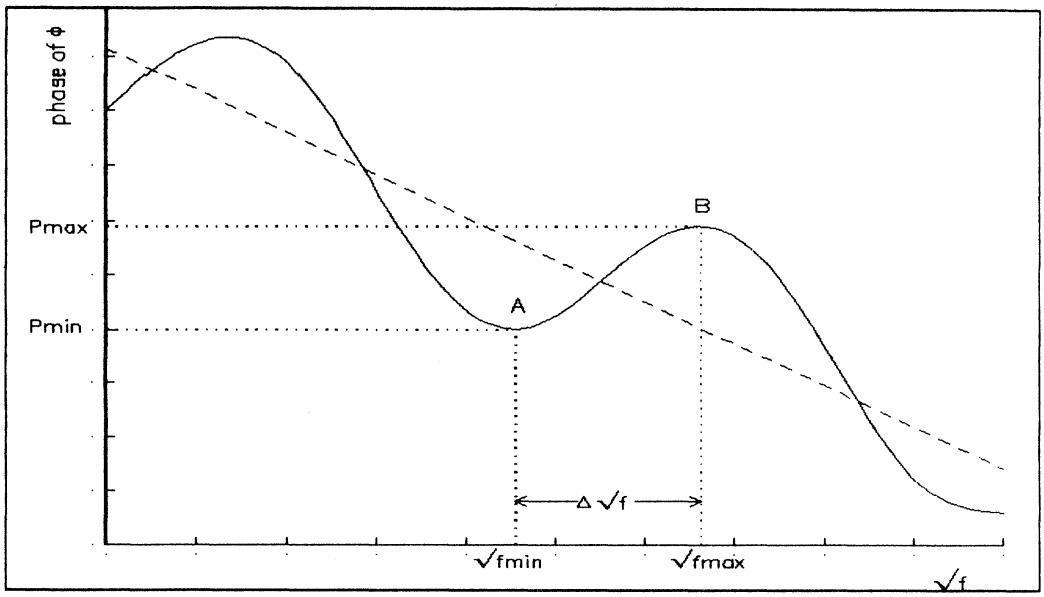

FIG. 3. Theoretical total phase Φ vs $f^{1/2}$ for thin-film samples described by Eqs. (7) and (8).

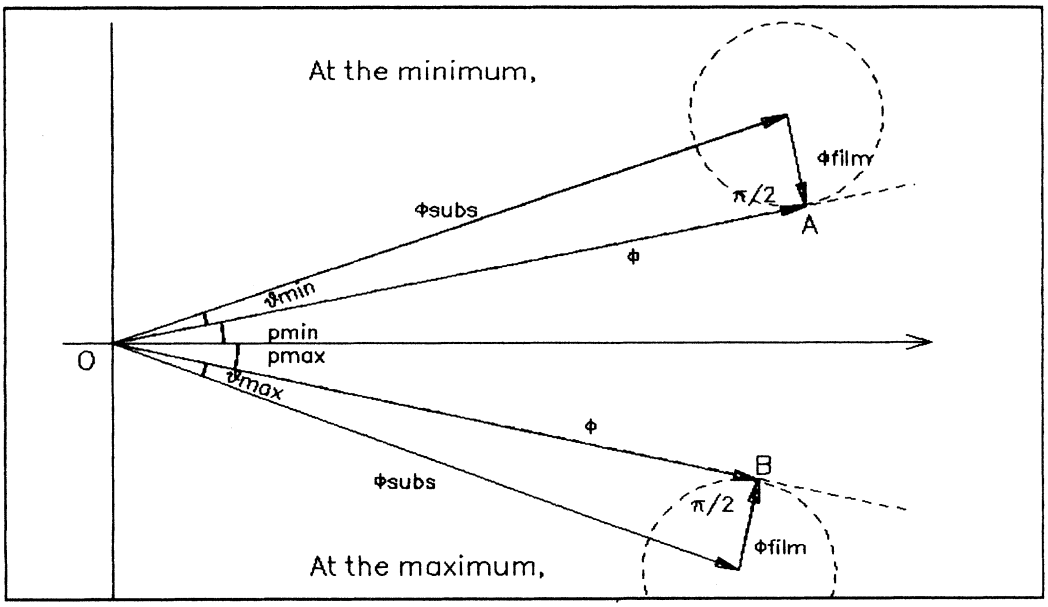

FIG. 4. The maximum and minimum of the phase occur when Φ is perpendicular to Φ_{film}.

$$\frac{\partial\ \text{phase}(\Phi_{\text{film}})}{\partial f^{1/2}}=\frac{-\pi+\theta_{\max}+\theta_{\min}}{\Delta f^{1/2}}+\frac{\partial[\text{phase}(\Phi_{\text{subs}})]}{\partial f^{1/2}}\ . \tag{13}$$

We must express $\theta_{\max}$ and $\theta_{\min}$ explicitly. Geometry tells us that

$$\theta_{\max}=\text{phase}(\Phi)-\text{phase}(\Phi_{\text{subs}}) \tag{14a}$$

at B of Fig. 3 and

$$\theta_{\min}=\text{phase}(\Phi_{\text{subs}})-\text{phase}(\Phi) \tag{14b}$$

at A of Fig. 3, leading to

$$\theta_{\max}+\theta_{\min}=-\frac{\partial[\text{phase}(\Phi_{\text{subs}})]}{\partial f^{1/2}}\Delta f^{1/2}+(P_{\max}-P_{\min})\ . \tag{15}$$

Substituting Eq. (15) back into (13) gives

$$\frac{\partial[\text{phase}(\Phi_{\text{film}})]}{\partial f^{1/2}}=\frac{-\pi\pm(P_{\max}-P_{\min})}{\Delta f^{1/2}}\ , \tag{16}$$

where the minus sign is introduced to take care of the situation when we meet the maximum before we meet the minimum as $f^{1/2}$ is increased. Using (10a),

$$\frac{\partial[\text{phase}(\Phi_{\text{film}})]}{\partial f^{1/2}}=\left[-\frac{y_0}{\chi_1^{1/2}}-\frac{z_0}{\chi_0^{1/2}}\right]\pi^{1/2}\ . \tag{17}$$

Fixing z_0 and sweeping the probe beam (i.e., varying y_0 from y_{01} to $y_{01}+\Delta y_0$), we obtain

$$\Delta\left[\frac{\partial[\text{phase}(\Phi_{\text{film}})]}{\partial f^{1/2}}\right]=-\Delta y_0\left[\frac{\pi}{\chi_1}\right]^{1/2}\ . \tag{18}$$

If the film is so thick that the contribution of the temperature field from the substrate is negligible, Eq. (18) is simplified to Eq. (6), which is especially accurate for low thermal-diffusivity measurements. Since the value on the left-hand side of the above equation can be measured directly using Eq. (16), we can obtain χ_1 readily by simply measuring Δy_0.

We would remark here that in most experiments χ_0 (0.19 cm^2s^{-1} for air) $\gg\chi_1,\chi_2$ and $y_0>z_0$. Equations (10a) and (10b) can be simplified to

$$\frac{\partial[\text{phase}(\Phi_{\text{film}})]}{\partial f^{1/2}}\approx-y_0\left[\frac{\pi}{\chi_1}\right]^{1/2}\ , \tag{19a}$$

$$\frac{\partial[\text{phase}(\Phi_{\text{subs}})]}{\partial f^{1/2}}\approx-y_0\left[\frac{\pi}{\chi_2}\right]^{1/2}\ . \tag{19b}$$

From the above equations thermal diffusivity of the substrate can be determined simultaneously from the same total phase-$f^{1/2}$ curves as for the film. The regression line of the periodic total phase-$f^{1/2}$ curve at certain y_0 is, in fact, the phase-$f^{1/2}$ relation of the substrate at that y_0 described by Eq. (10b). In a mirage measurement of thin films of low thermal diffusivity, we normally have $y_0>z_0$ and χ_0 (for air) $\gg\chi_1,\chi_2$, giving

$$\chi_1\left[\frac{\partial[\text{phase}(\Phi_{\text{film}})]}{\partial f^{1/2}}\right]^2=\chi_2\left[\frac{\partial[\text{phase}(\Phi_{\text{subs}})]}{\partial f^{1/2}}\right]^2\ . \tag{20}$$

In view of relation (16), and as χ_1 has already been found at this stage, the left-hand side is all known. Now $\partial[\text{phase}(\Phi_{\text{subs}})]/\partial f^{1/2}$ is simply the slope of the regression line of the phase-$f^{1/2}$ plot, and χ_2 can therefore be calculated using (20).

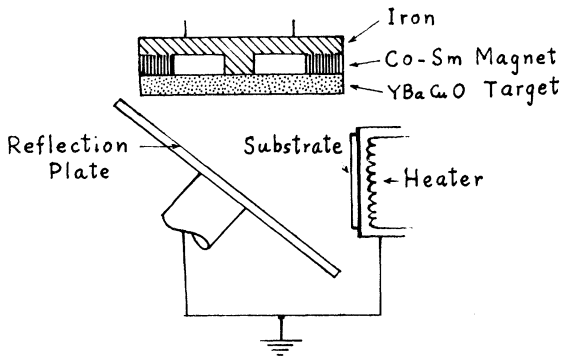

FIG. 5. Schematic diagram of the modified off-axis rf magnetron sputtering system used to prepare our thin-film sample.

In Sec. V, we shall apply our theory to evaluate the thermal diffusivity coefficients of both the film and the substrate using actual experimental data. In the meantime we shall briefly describe the method of fabricating our thin-film sample using a magnetron sputtering technique.

III. PREPARATION OF THE THIN-FILM SAMPLE

We attempt to employ the modified off-axis rf-magnetron sputtering method[13] to fabricate our thin film $YBa_2Cu_3O_{7-\delta}$ sample. The *in situ* growth of superconducting oxide thin films requires a relatively high deposition temperature (650–740 °C) in a mixture of oxygen and argon environment. The heater must be in good thermal contact to the substrate without evaporating any significant part of its components. The substrate temperature, which was kept at the value 680 °C during deposition, is measured using a Pt-Pt 87 wt. %, Ph 13 wt. % thermocouple, which is mounted through a hole drilled in a dummy Al_2O_3 substrate.

(305) $SrTiO_3$ single crystals with well-polished surfaces are used as substrates. The background pressure of the deposition system is pumped to less than 5×10^{-5} Pa by a turbo molecular pump. A mixture of 50% argon and 50% oxygen is used as sputter gas. The operating pressure is about 30 Pa. The incident rf power is set to about 100 W. Under the stated conditions, the deposition rate is found to be about 2 nm/min. In most cases the gas-grown films are cooled down directly to room temperature after deposition reaches a rate of about 80° per minute. The schematic diagram of the modified off-axis rf magnetron sputtering system is shown in Fig. 5. During sputter deposition of the thin-film, oxygen ions are accelerated to the deposited film and the bombardment can cause severe damage of the film, as pointed out by several authors (e.g., Clark *et al.* in Ref. 14). It is therefore important to provide a sufficient thermalization for the accelerated particles. Such a factor is taken into account by adjusting the sputter geometry. A reflection plate is added, inclined 45° to the surface of the target, as shown in Fig. 5. This reflection plate further decreases the ion bombardment by negative ions emerging from the cathode. Since it is grounded, it provides a well-defined counter electrode for the magnetron discharge. On the way between the reflection plate and the substrate, both on ground potential, the particles are not accelerated any more and thus should be very well thermalized. One good thin film of size 10×10 mm^2, of thickness 60 nm, is chosen for our diffusivity analysis. Note that a reflection plate is mounted. EDX measurement is carried out to

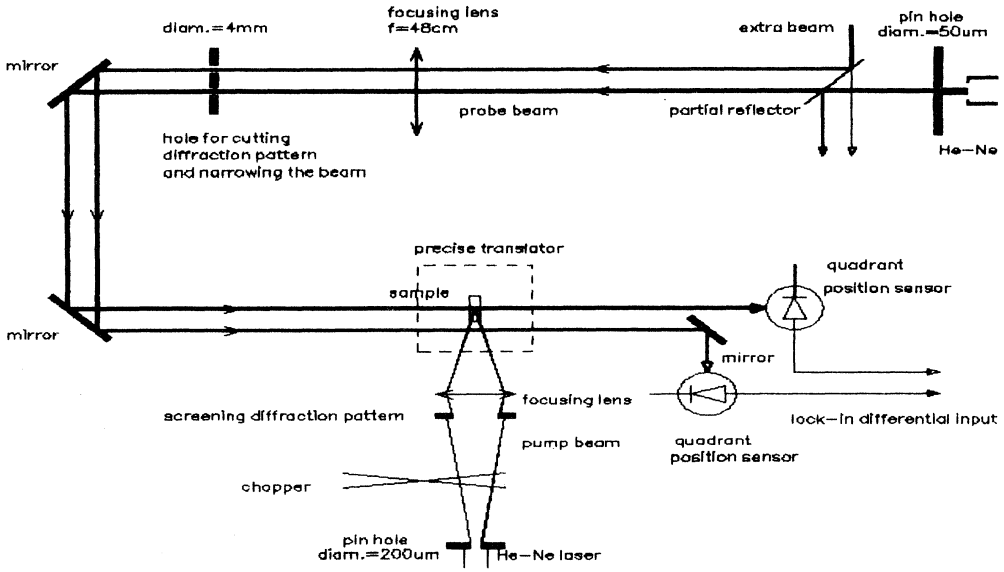

FIG. 6. Configuration of the setup for the mirage experiment. The pump beam is reflected onto the sample by a mirror (not shown) mounted on the precise translator table. y_0 and z_0 can be changed by translating the pump beam and the sample relative to the probe beam. The extra beam is set for mechanical noise rejection, and it does not suffer mirage deflection.

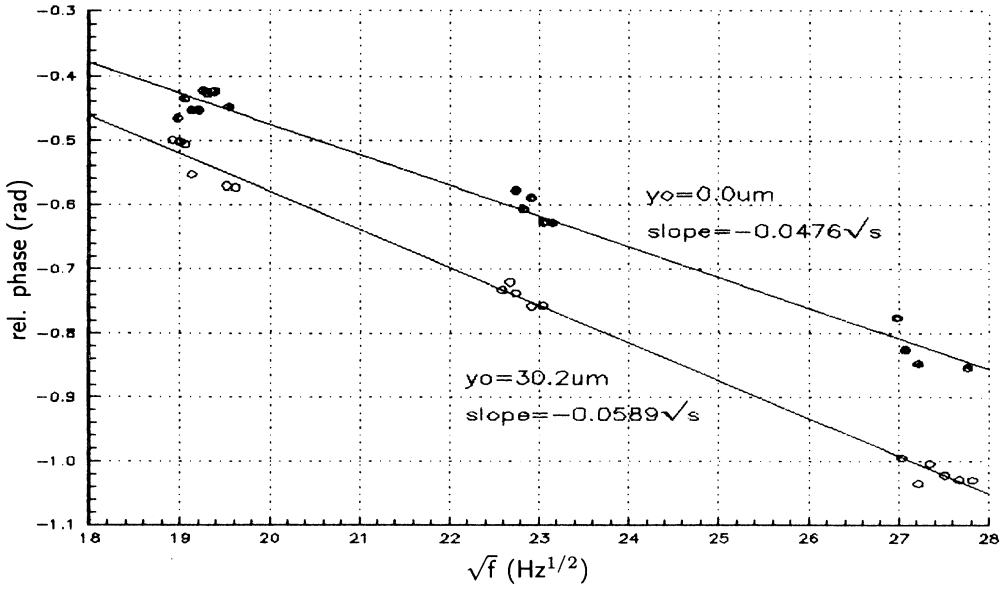

FIG. 7. Phase-$f^{1/2}$ curves for an iron slab sample with $\Delta y_0 = 30.2\ \mu$m. Δ slope $= -0.0113\ s^{1/2}$.

measure the atomic ratio on about 10 spots on an area of $30 \times 30\ \mu m^2$; the atomic ratio of Y:Ba:Cu is found to be very close to 1:2:3.

IV. THERMAL-DIFFUSIVITY MEASUREMENT

Transverse photothermal deflection configuration is employed to carry out our diffusivity measurement (Fig. 6). The pump and probe beams are both He-Ne lasers with powers 4.9 mW and 0.03 mW, and spot sizes 40 μm and 70 μm, respectively. The separation of the probe from the pump beam, i.e., the distance y_0, could be changed by a precise translator on which the sample is mounted, while the precise translator is adjusted by a digital controller (Oriel, model No. 18008) with a minimum increment of 0.1 μm. The mirage effect is detected by a quadrant position sensor (UDT, with an amplifier module—model No. 301DIV). We operate an

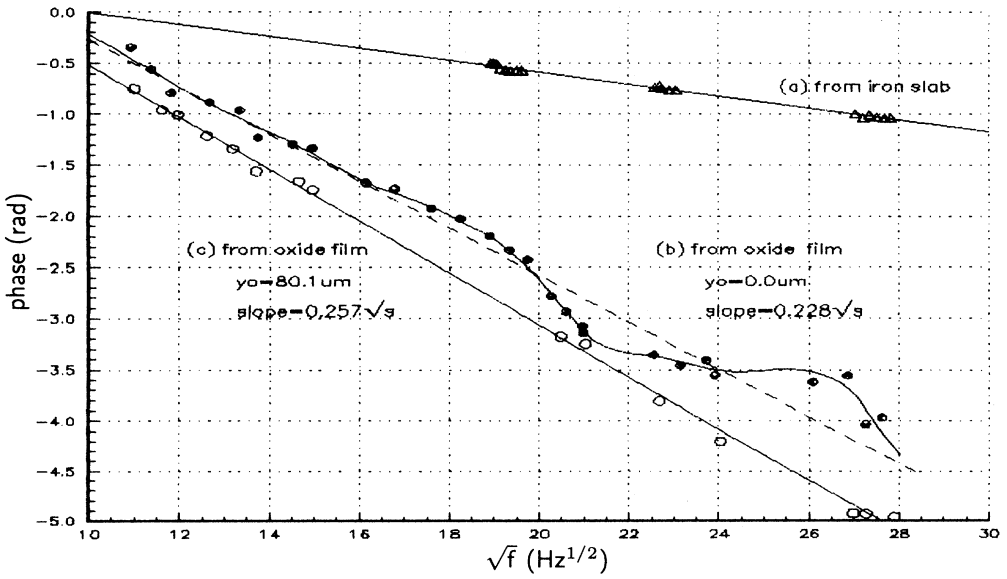

FIG. 8. The phase-$f^{1/2}$ graphs for a pure iron slab (a). Using an iron slab with an oxide thin as another sample and with $y_0 = 0$, we have a periodic graph (b). When the probe beam is "far" ($y_0 = 80.1\ \mu$m) from the pump beam the graph of the oxidized sample is linear again.

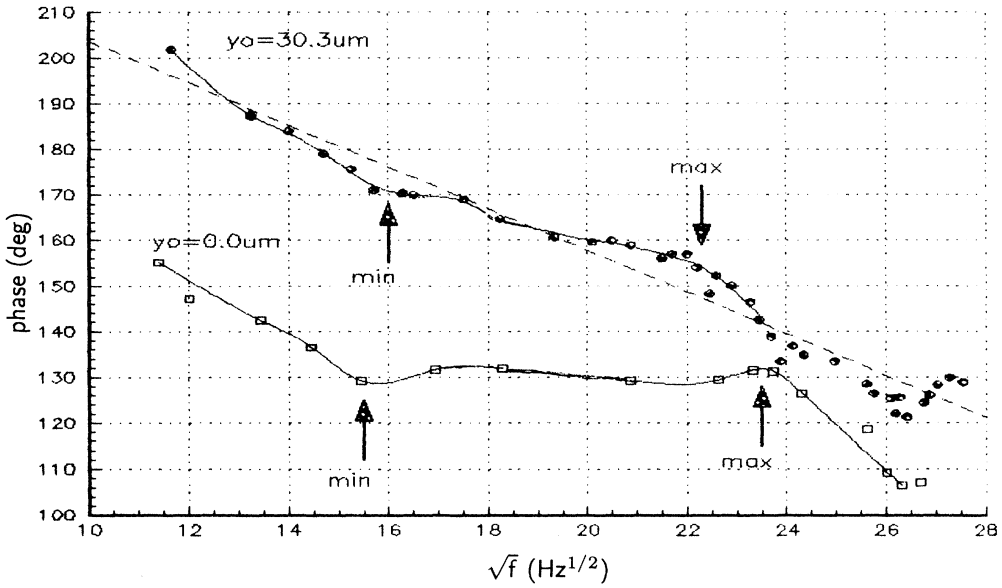

FIG. 9. Phase-$f^{1/2}$ curves of the superconducting sample with the probe beam along the c axis of the single crystal. Changing y_0 to 30.3 μm, another curve is shown.

extra He-Ne laser beam running along with the probe at about 7 mm apart and passing the same optical pieces as the probe beam. This extra beam experiences the same mechanical disturbances as the probe, but suffers no mirage effect as it is set to be too far from the pump beam. Finally the beam reaches a quadrant position sensor (the same model as that stated before) beside that for the probe. Signals from the two position sensors are fed into the differential input of a lock-in amplifier (SR 530) for phase measurement and noise rejection. We find that the extra beam performs very well in stabilizing the dc lock-in output. To measure the thermal diffusivity along the b axis of the single-crystal thin film, the probe beam is set to run perpendicularly to the b axis. For c axis measurement, the probe beam runs along the b axis. The whole experiment is aligned on an optical table (Newport model No. RS 2000) to screen out mechanical disturbances.

Before we use our theoretical expressions derived in Sec. II to analyze our experimental results, we will first check the validity of some crucial points with presently observed and known experimental data. First we make an iron slab with a size similar to the thin film and repeat the mirage-detection experiment stated, and plot two phase-$f^{1/2}$ curves with $\Delta y_0 = 30.2$ μm (Fig. 7). The difference in the two slopes (Δ slope) is found to be 0.0113 $s^{1/2}$. Putting the values of Δy_0 and Δ slope into Eq. (6), the thermal diffusivity of iron thus determined is 0.224 $cm^2 s^{-1}$, in good agreement with the established reported value of 0.227 $cm^2 s^{-1}$.[14] We follow up our verification of our theoretical deduction by also measuring the phase-$f^{1/2}$ relation of an iron slab already covered with an oxide layer with $y_0 = 0$ μm. The phase-$f^{1/2}$ plot has a periodic structure, as indicated by curve (b) of Fig. 8. The dotted straight line is the regression line having a slope of -0.228 $s^{1/2}$. We repeat the mirage experiment with the probe beam far away from the pump beam—$y_0 = 80.1$ μm. We expect the T_{film} to contribute very little for such large value of y_0 as $\chi_{\text{Fe}} \gg \chi_{\text{oxide}}$ and the periodic structure should disappear according to our theory. The measured phase-$f^{1/2}$ graph is found indeed to be a straight line [line (c) of Fig. 8]. For comparison, the phase-$f^{1/2}$ relation for the "pure" iron slab is also shown as curve (a) in the same figure without any period observed.

TABLE I. Parameters for the calculation of anisotropic thermal diffusivity of $YBa_2Cu_3O_{7-x}$ thin film.

Parameter	c-axis measurement		b-axis measurement	
y/μm	0.0	30.0	90.1	120.1
$p_{\max}$/deg	131.6±1	154.5±1	143.5±1	158.8±1
$p_{\min}$/deg	128.7±1	170.5±1	147.2±1	158.1±1
$f^{1/2}_{\max}/\text{Hz}^{1/2}$	23.5±0.1	22.3±0.1	26.5±0.1	24.8±0.1
$f^{1/2}_{\min}/\text{Hz}^{1/2}$	15.5±0.1	16.0±0.2	14.0±0.1	14.1±0.1

V. RESULTS AND ANALYSIS

Total phase-$f^{1/2}$ curves of our film-substrate composite sample described in Sec. III at different y_0 obtained in the c-axis measurement are shown in Fig. 9, where the two curves correspond to $y_0=0.0$ and 30.3 μm. We can identify two maxima and minima on these two curves within the range 12 $Hz^{1/2}<f^{1/2}<26$ $Hz^{1/2}$. We recorded the parameters $P_{max}, P_{min}, f_{max}^{1/2}, f_{min}^{1/2}$ and the results are presented in Table I. The value of χ_1 can then be evaluated readily using such data and χ_1 turns out to be 0.0012 $cm^2 s^{-1}$ along the c axis. Rotating the sample by 90°, we repeated the b axis measurements and the results are also presented in the table.

We now draw the regression line through the data points for the case $y_0=30.3$ μm. Since there are data points covering more than one cycle, the slope of the regression line is rather accurate. Putting the slope of this regression line, and $\partial[\text{phase}(\Phi_{film})]/\partial f^{1/2}$ calculated using Eq. (16) and χ_1 (=0.0012 $cm^2 s^{-1}$) into Eq. (20), we find that χ_2 is 0.053 $cm^2 s^{-1}$. This value is very close to that reported for the substrate $SrTiO_3$, which is 0.05 $cm^2 s^{-1}$.[15–17] Such a result supports the validity of our approach. Similarly the thermal diffusivity along the b axis can be calculated from Eqs. (16) and (18) using the data in Table I, and χ_1 turns out to be 0.022 $cm^2 s^{-1}$, which is practically the same value reported earlier; see Refs. 4, 5, and 18. The anisotropy factor is then 18 for our crystal, which is in good agreement with the anisotropy in thermal conductivity, 17.[19] For the sake of comparison and further analysis, we list in Table II the results of thermal-diffusivity measurements for $YBa_2Cu_3O_{7-\delta}$ that have been published, to the best of our knowledge, together with some relevant parameters or remarks. Note that the transient grating method gives $\chi_1=0.0028$ $cm^2 s^{-1}$ for a 220-nm-thick Y-123 film on the MgO substrate along the c axis in 1992.[4] More recently, χ_1 is found to be 0.0026 $cm^2 s^{-1}$ for a slightly thinner (190-nm)

TABLE II. Lists the thermal diffusivity measurements performed on $YBa_2Cu_3O_{7-\delta}$ taken from literature and our work.

Thermal diffusivity χ_1 at 300 K ($cm^2 s^{-1}$)	Sample and remarks	Method	Ref.
0.0017	0.5 mm thick with mixed orientation	flash method	21
0.009	1 mm thick with mixed orientation		22
0.007	Pellets with mixed orientation	Photoacoustic phase-lag and flash methods	23
0.012	1mm thick pellets with mixed orientation		24
0.046~0.071	Thin films on ZrO_2 substrate, no thickness specified; variation due to differences in annealing conditions	Mirage method	7
0.023 in ab plane	0.05–0.35-μm-thick thin films on MgO, c oriented	Transient grating	18
0.023 in ab plane 0.0028 along c axis	0.22-μm-thick thin films on MgO substrate, c oriented	transient grating	4
On MgO: 0.023 in ab plane, 0.0026 along c axis; on $SrTiO_3$ 0.022 in ab plane, 0.0026 along c axis	190-nm-thick thin film on MgO or $SrTiO_3$ substrate, c oriented	Transient grating	5
0.0012 along c axis	$3\times3\times1$ mm^3 single crystal	pyroelectric impulse response	20
0.022 along b axis 0.0012 along c axis	60-nm-thick thin film on (305) $SrTiO_3$ substrate	mirage method based on the present model including contributions from film and substrate	This work

film on both MgO and $SrTiO_3$ substrates along the c axis.[5] We expect that there is some contribution to the observed overall thermal diffusivity from the substrate, in particular when the film is too thin. In our analysis, we subtract the contribution from the substrate and obtain a smaller value of 0.0012 $cm^2 s^{-1}$. This value is equal to that obtained by the pyroelectric impulse response using a single crystal (without substrate).[20]

VI. CONCLUSIONS

(1) We derive explicit expression for the thermal diffusivity for film-substrate composite samples by including the contributions from the film as well as the substrate to the temperature field at the probe beam position. Our theoretical expression, Eq. (18), requires that measuring the phase of deflection at two positions (y_0) over a range of pumping frequency is sufficient to determine the diffusivity of the film χ_1. Using the regression line of the phase-$f^{1/2}$ plot, we can simultaneously evaluate the diffusivity of the substrate employing Eq. (20) with the knowledge of χ_1 just found.

(2) We are guided by our theoretical analysis to carry out the mirage experiment with an extra thin film on a standard substrate. Since the film sample used by researchers employing the transient grating method is about 200 nm, we fabricate a single-crystal $YBa_2Cu_3O_{7-\delta}$ film with thickness significantly smaller than 200 nm, in order to check our theory. The film sample is prepared by the off-axis magnetron sputtering method and is found to have a size of 10×10 mm^2 and a thickness of only 60 nm.

(3) To check the validity of the theory, we measure the magnitudes and phases of the mirage signals of a pure iron slab as well as a similar slab that has an oxide film on top. We varied the distance between the pump and probe beams purposely in order to see whether the periodic structure would occur and disappear—the phase-$f^{1/2}$ relation behaves as predicted by theory.

(4) We then perform the key mirage experiment employing our $YBa_2Cu_3O_{7-\delta}$ film sample on $SrTiO_3$ at 300 K, and measure the thermal diffusivity along the c and b axes. The χ value along the c axis is identical to that measured by the pyroelectric impulse response method (employing a single crystal with no substrate), but is about 50% of that measured by the transient grating method. While we do not question the accuracy of the previous result obtained by the TG method, the temperature field at the point of observation might have been contributed by both the film and the substrate. We note also that χ value along the b axis is practically identical to that obtained by the TG method.

(5) The TG method employed by Marshall *et al.* possesses a number of advantages: It is a time-domain technique for direct measurement of dynamic phenomena. It also provides a direct, but noncontacting and nondestructive, means of evaluating thin-film and interface properties such as thermal boundary resistance.[5] The power density required is relatively low (~ 10 μW). By aligning the grating wave vector suitably relative to the sample, anisotropic measurements can be made. Furthermore, it can be performed at low temperatures and requires no coupling medium around the sample. Moreover, the level of information is substantially higher than that of the mirage method. However, a number of parameters (such as the complex refractive indices of the film and substrate, and thermal diffusivity of the substrate) must be known before numerical fitting can be carried out to evaluate the thermal diffusivity along the surface normal. The advantages are that the mirage technique is cheaper and easier to setup than a picosecond transient grating experiment. But it is sensitive to air current and mechanical disturbances. However, in our actual setup, these influences are largely screened out by the differential technique and by using a high-quality optical table. In situations where exceptionally high signal-to-noise ratio is required, the boxcar integration technique can be employed. With the development for the mirage detection reported here, it appears that such as photothermal method is a reliable and relatively easy technique to measure the thermal diffusivity of thin films on a substrate as well as other types of samples. Using better basic equipment, as reported here, we believe more accurate results can be achieved.

(6) Anisotropic thermal diffusivity of a superconductor, even in its normal state, is an important physical quantity that can give a hint as to the nature of superconductivity. The small χ value along the c axis, as compared to that along the ab plane found here, indicates that superconductivity originates from a phonon-mediated mechanism, namely, a modified BCS type of charged-pair condensation.

[1]K. C. Tsui, P. C. W. Fung, H. L. Tam, and G. O. Walker, J. Phys. Chem. Solids **52**, 979 (1991).

[2]S. J. Hagen, Z. Z. Wang, and N. P. Ong, Phys. Rev. B **40**, 9389 (1989).

[3]I. M. Fishman, C. D. Marshall, J. S. Meth, and M. D. Fayer, J. Opt. Soc. Am. B **8**, 1880 (1991).

[4]C. D. Marshall, I. M. Fishman, R. C. Dorfman, C. B. Eom, and M. D. Fayer, Phys. Rev. B **45**, 10 009 (1992).

[5]C. D. Marshall, A. Tokmakoff, I. M. Fishman, C. B. Eom, Julia M. Phillips, and M. D. Fayer, J. Appl. Phys. **73**, 850 (1993).

[6]H. J. Eichler, P. Gunter, and D. W. Phol, *Laser Induced Dynamic Gratings* (Springer-Verlag, Berlin, 1986).

[7]X. Zhang, C. Gam, Z. Xu, S. Zhang, and H. Zhang, *Photoacoustic and Photothermal Phenomena II* (Springer-Verlag, Berlin, 1990), p. 205.

[8]G. Suber, M. Bertolotti, C. Sibilia, and A. Ferrari, Appl. Opt. **27**, 1807 (1988).

[9]A. Salazar, A. Sanchez-Lavega, and J. Fernandez, J. Appl. Phys. **69**, 1216 (1991).

[10]P. K. Kou, M. J. Lin, C. B. Ryes, L. D. Favro, R. L. Thomas, D. S. Kim, S. Y. Zhang, L. J. Inglehart, D. Fournier, A. C. Boccara, and N. Yacoubi, Can. J. Phys. **64**, 1165 (1986).

[11]W. B. Jackson, N. M. Amer, A. C. Boccara, and D. Fournier,

Appl. Opt. **20**, 1333 (1981).
[12]G. Suber, M. Bertolotti, C. Sibilia, A. Ferrari, and F. Genel Ricciardiello, J. Thermal Analysis **32**, 1039 (1987).
[13]J. Gao, B. Häuser, and H. Rogalla, J. Appl. Phys. **67**, 2512 (1990).
[14]G. J. Clark, A. D. Marwich, R. H. Kock, and R. B. Laibowitz, Appl. Pats. Lett. **51**, 139 (1987).
[15]David R. Lide, *CRC Handbook of Chemistry and Physics,* 72nd ed. (CRC, Boca Raton, 1991).
[16]Y. S. Touloukian, R. W. Powell, C. Y. Ho, and P. G. Klemens, *Thermal Conductivity: Nonmetallic Solids. Thermophysical Properties of Matter* (Plenum, New York, 1970).
[17]Y. S. Touloukian, R. W. Powell, C. Y. Ho, and M. C. Nicolaou, *Thermal Diffusivity: Thermophysical Properties of Matter* (Plenum, New York, 1973).
[18]C. D. Marshall, I. M. Fishman, and M. D. Fayer, Phys. Rev. B **43**, 2696 (1991).
[19]S. C. Cao, D. M. Zhang, and D. L. Zhang, Phys. Rev. B **44**, 12 571 (1991).
[20]S. B. Peralta, I. A. Vitkin, K. Ghandi, A. Mandelis, W. Sadowski, and E. Walker, *Photoacoustic and Photothermal Phenomena II* (Ref. 7), p. 211.
[21]J. V. Armstrong, M. McLoughlin, J. G. Luney, and J. M. D. Coey, Superconduct. Sci. Technol. **4**, 89 (1991).
[22]S. B. Peralta, Z. H. Chen, and A. Mandelis, Appl. Phys. A **52**, 289 (1991).
[23]L. Gomez, M. M. F. Vieira, S. L. Baldochi, N. B. Lima, M. A. Novak, N. D. Vieira, Jr., S. P. Morato, A. J. P. Braga, C. L. Cesar, A. F. S. Penna, and J. M. Filho, J. Appl. Phys. **63**, 5044 (1988).
[24]S. B. Peralta, Z. H. Chen, and A. Mandelis, Ferroelectrics **118**, 425 (1991).